Simultaneous frequency and T2 mapping, applied to thermometry and to susceptibility-weighted imaging

Cheng-Chieh Cheng[1], Chang-Sheng Mei[2], Pelin Aksit Ciris[3,4], Robert V. Mulkern[4,5], Mukund Balasubramanian[4,5], Hsiao-Wen Chung[1], Tzu-Cheng Chao[6], Lawrence P. Panych[3,4], and Bruno Madore[3,4]

[1]Graduate Institute of Biomedical Electronics and Bioinformatics, National Taiwan University, Taipei, Taiwan, [2]Department of Physics, Soochow University, Taipei, Taiwan, [3]Department of Radiology, Brigham and Women's Hospital, Boston, MA, United States, [4]Harvard Medical School, Boston, MA, United States, [5]Department of Radiology, Boston Children's Hospital, Boston, MA, United States, [6]Department of Computer Science and Information Engineering, National Cheng-Kung University, Tainan, Taiwan

Target audience: Researchers or clinicians involved in situations that may benefit from both T_2 and field mapping, such as thermometry or susceptibility imaging.

Purpose: Quantitative T_2 maps and field maps can provide rich clinically-relevant information. In brain exams, T_2 mapping is key to tumor detection while field mapping enables susceptibility imaging, to detect iron accumulation, which might be indicative of conditions such as bleeding, Parkinson's disease, Alzheimer's disease, or multiple sclerosis. In thermometry, field mapping enables temperature measurements through the proton resonance frequency shifting effect while T_2 mapping may provide a complementary means of detecting heat-induced damage. Different pulse sequences are typically required to obtain T_2 and field information: a spin-echo (SE) based sequence for T_2 and a gradient-echo (GRE) based sequence for field mapping. The need for two different sequences tends to prevent T_2 and field information from being acquired together. Although, methods based on asymmetrical spin-echoes have been proposed to capture both types of information, such sequences tend to be relatively slow[1]. Here, we describe application of a steady-state multi-pathway GRE sequence and associated reconstruction algorithm to capture both T_2 and field maps with relatively-fast scan time, and present results in both susceptibility+T_2 and thermometry+T_2 applications.

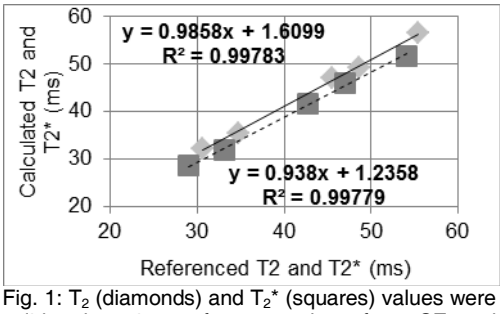

Fig. 1: T_2 (diamonds) and T_2* (squares) values were validated against reference values from SE and GRE scans.

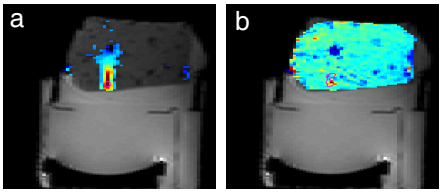

Fig. 2 Ultrasound heating of ex-vivo tissues, (a) shown with temperature overlay and (b) with T_2 overlay.

Methods: FID and spin-echo signals undergo different transverse relaxation processes. R_2 and R_2' in Eq.1 and Eq.2 represent irreversible and reversible decay rates, respectively, where $T_2 = 1/R_2$ and $T_2^* = 1/(R_2+R_2')$. MR signals may change with either (R_2+R_2') or (R_2-R_2') depending on whether the reversible decay is evolving (e.g., an FID signal) or devolving (e.g., SE signal on its way to formation). The present work involves a 'dual echo in the steady state' (DESS) sequence, which samples both an FID signal (S_j^+) and a SE-like signal (S_j^-) at several different echo times TE_j^+ and TE_j^-, respectively. The following expressions are fitted to obtain 4 unknowns (S_0^+, S_0^-, R_2 and R_2'): $S_j^+ = S_0^+ e^{-(R_2+R_2')\times TE_j^+}$, $S_j^- = S_0^- e^{-(R_2-R_2')\times TE_j^-}$ [Eq. 1]. T_2 and T_2* can then be determined from R_2 and R_2'. Field maps are obtained by fitting to the linear phase evolution with TE_j^+ and TE_j^-, and these maps are then converted into either susceptibility or temperature maps.

The assumption of an exponential T_2* decay is based on Lorentzian intra-voxel frequency distributions, a condition that is frequently not met[2]. Deviations from a Lorentzian distribution are not considered in the model above, which in turn causes errors ion measured T_2 values. The model below, extends the model above, by incorporating the possibility that intra-voxel frequency distributions may be better characterized with Gaussian functions, as recently found in the brain[2], and was employed for the brain data presented here: $S_j^+ = S_0^+ e^{-(R_2+R_2')\times TE_j^+ - \sigma TE_j^{+2}}$, $S_j^- = S_0^- e^{-(R_2-R_2')\times TE_j^- + \sigma TE_j^{-2}}$ [Eq. 2]. These equations are fitted to obtain S_0^+, S_0^-, R_2, R_2', and σ. Locations with σ≈0 represent tissues where the simpler Eq. 1 was sufficient to model the decay, and σ≠0 to tissues where the extended model of Eq. 2 proved useful.

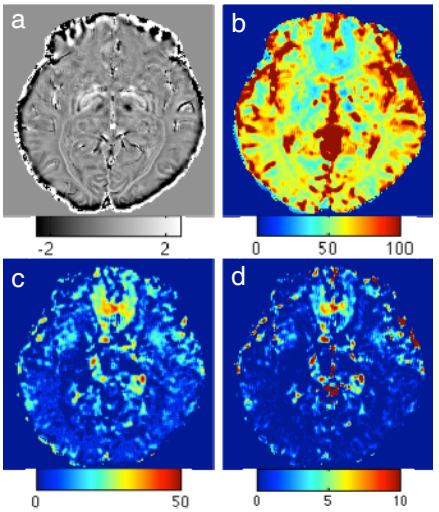

Fig. 3 (a) internal field perturbation (in Hz), (b) fitted T_2 map (in ms) with extra consideration of σ, (c) σ map, and (d) T_2 difference (in %).

Results: The method was validated against regular SE and GRE scans using a 5-tube phantom with varying amounts of manganese sulfate (3T, FA=25°, TR=25ms, TE^+/TE^- = 5.5, 9.8, 14.0, 18.3 / 6.8, 11.0, 15.2, 18.3 ms, 399Hz/px, FOV=18×18cm, 64×128pixels). Correct values for T_2 and T_2* were obtained (Fig. 1).

For thermometry, bovine tissue was heated using ultrasound. Fig. 2a shows temperature and Fig. 2b shows T_2 overlaid on structural images (3T, FA=35°, TR=20.6ms, TE^+/TE^- = 3.4, 7.6, 11.8, 15.9 / 4.7, 8.8, 13.0, 17.2 ms, 399Hz/px, FOV=20×20cm, 128×128pixels). A red outline shows the extent of heat-induced damage as measured with a temperature dose threshold of 240CEM_{43} (Fig. 2a) or of 15% T_2 change (Fig. 2b). Time-averaged T_2 away from focus was measured at 43.6 ms, as expected for muscle tissue at 3T.

For brain imaging, the internal field perturbation and a T_2 map (obtained using Eq. 2) are shown in Fig. 3a and 3b, respectively (3T, 3D sequence, FA=25°, TR=50ms, TE^+/TE^- = 4.0, 11.9, 19.8, 27.7, 35.6, 43.6 / 6.4, 14.4, 22.3, 30.2, 38.1, 46.0 ms, 200Hz/px, FOV=19.2×19.2×7.2cm, 128×128×36pixels). A map of σ and the change in T_2 values between Eq. 1 and Eq. 2 (as a percentage) are shown in Fig. 3c and 3d, respectively. In Fig. 3c higher σ values tend to indicate higher field inhomogeneities and T_2 errors in Fig. 3d.

Discussion and Conclusion: Simultaneous T2 and field mapping can be achieved using the proposed method, and a more elaborate fitting procedure that does not assume a Lorentzian intra-voxel frequency distribution may prove especially useful in non-homogeneous field regions.

References: [1] Ma J, Wehrli. JMR B 1996;111:61-9. [2] Mulkern et al. MRM 2014, doi: 10.1002/mrm.25365.

Support from NIH grants R01CA149342, P41EB015898 and R01EB010195 is acknowledged.